Ultrafast domain wall motion in ferrimagnets induced by magnetic anisotropy gradient

W. H. Li,[1] Z. Jin,[1] D. L. Wen,[1] X. M. Zhang,[1] M. H. Qin,[1,*] and J.-M. Liu[2]

[1]*Guangdong Provincial Key Laboratory of Quantum Engineering and Quantum Materials and Institute for Advanced Materials, South China Academy of Advanced Optoelectronics, South China Normal University, Guangzhou 510006, China*

[2]*Laboratory of Solid State Microstructures and Innovative Center for Advanced Microstructures, Nanjing University, Nanjing 210093, China*

(Received 14 October 2019; revised manuscript received 23 December 2019; published 16 January 2020)

The ultrafast magnetic dynamics in compensated ferrimagnets not only is similar to antiferromagnetic dynamics but, more importantly, opens new opportunities for future spintronic devices [Kim *et al.*, Nat. Mater. **16**, 1187 (2017)]. One of the most essential issues for device design is searching for low-power-consuming and high-efficient methods of controlling the domain wall. In this work, we propose to use the voltage-controlled magnetic anisotropy gradient as an excitation source to drive the domain wall motion in ferrimagnets. The ultrafast wall motion under the anisotropy gradient is predicted theoretically based on the collective coordinate theory, which is also confirmed by the atomistic micromagnetic simulations. The antiferromagnetic spin dynamics is realized at the angular momentum compensation point, and the wall shifting has a constant speed under small gradients and can be slightly accelerated under large gradients due to the broadened wall width during the motion. For nonzero net angular momentum, the Walker breakdown occurs at a critical anisotropy gradient significantly enhanced by the second anisotropy and interfacial Dzyaloshinskii-Moriya interaction, which is highly appreciated for further experiments, including the materials selection and device geometry design. More importantly, this work unveils a low-power-consuming and highly efficient method of controlling the domain wall in ferrimagnets, benefiting future spintronic applications.

DOI: 10.1103/PhysRevB.101.024414

I. INTRODUCTION

Antiferromagnetic materials show fast magnetic dynamics and produce nonperturbing stray fields, attributed to their zero magnetization and ultralow susceptibility. These advantages make them promising candidates for the next generation of high-density and high-speed spintronic devices [1–5]. However, the magnetic field immunity of antiferromagnetic materials also hinders the detection and manipulation of magnetic states [6–8]. Thus, it is still challenging to experimentally study the antiferromagnetic spin dynamics, although several stimuli have been predicted to drive the fast domain wall motion in earlier theoretical works [9–18]. Therefore, a reliable and direct detection of the magnetic states remains a common issue for antiferromagnetic spintronic researchers.

To overcome this deficiency, an immediate alternative strategy is to consider ferrimagnetic (FiM) systems where the fast magnetic dynamics in the vicinity of angular momentum compensation temperature T_A can be achieved [19], at which the net momentum vanishes while the net magnetic moment is nonzero. It has been theoretically predicted and experimentally confirmed that the FiM dynamics at T_A is similar to the antiferromagnetic dynamics. More importantly, the magnetic states of a FiM system at T_A can be effectively detected and addressed through the magnetoelectric [20–22] and magneto-optical [23] responses, benefiting from their nonzero magnetic moment, and are thus highly appreciated.

In fact, magnetic-field- and electrical-current-driven fast domain wall motions in angular-momentum-compensated ferrimagnets have been experimentally reported, respectively [19,24–26]. Also, the Walker breakdown field, under which the domain wall begins to precess and reaches a threshold speed, is significantly increased and the domain wall mobility is extensively enhanced when the net angular momentum approaches zero. At T_A, the Walker field diverges and the domain wall speed keeps increasing linearly with field due to the excluded Walker breakdown, exactly the same as in antiferromagnets. For example, a domain wall speed as high as $\sim 20\,\mathrm{km\,s^{-1}\,T^{-1}}$ was reported at T_A in rare-earth 3*d* transition-metal ferrimagnets [19]. Thus, the magnetic dynamics in ferrimagnets at T_A not only provides equivalent information for antiferromagnetic spin dynamics but, more importantly, opens new opportunities for future spintronic devices.

On the other hand, searching for well-controlled and low-power-consumed methods to modulate FiM domain walls is one of the most important issues for spintronic device operation, noting that the shortcomings of these proposed schemes may be detrimental for future applications. For instance, the characteristic dispersion of the magnetic field generally limits the density of ferrimagnetic elements and hinders further optimization of device dimension. Moreover, some of the electrical-current-related schemes normally generate Joule heating and unnecessary energy loss, significantly affecting the data transportation process where a stable operating temperature is beneficial. Along this line, electric field control could be highly preferred [27], to be explained in detail below.

*qinmh@scnu.edu.cn

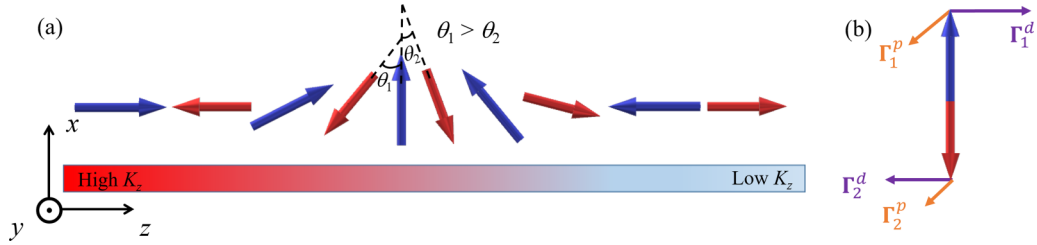

FIG. 1. (a) Illustration of a domain wall in ferrimagnetic nanowire under an anisotropy gradient. Here the asymmetry of the domain wall center is exaggerated. (b) A schematic depiction of torques acting on the central spins of the domain wall.

First, numerous experiments have revealed the voltage control of magnetism. For example, the voltage-induced magnetic anisotropy gradient has been experimentally reported in magnetic heterostructures through elaborate structural design [28–30]. Under such a gradient, the magnetic domain wall tends to move towards the low-anisotropy side in order to save free energy. As a matter of fact, the anisotropy gradient has been proven to efficiently drive the skyrmion motion and antiferromagnetic domain wall motion [31–33], and this scheme could be also utilized to control the FiM domain wall motion. More importantly, this alternative scheme is promising for future spintronic applications, considering its low energy costs and the high operating efficiency. However, as far as we know, few works on this subject have been reported, while the dynamics of FiM domain walls under anisotropy gradient is certainly an urgent topic to be understood in order to provide instruction for future experiments and promote the application process for spintronics.

In this work, we study the domain wall dynamics of ferrimagnets under an anisotropy gradient using the collective coordinate theory and atomistic Landau-Lifshitz-Gilbert (LLG) simulations. It is demonstrated that the wall speed and precession direction depend closely on the net angular momentum. At the angular momentum compensation point, the Walker breakdown vanishes and the wall moves at a maximal speed, similar to the case of antiferromagnetic dynamics. It will be shown that the wall continues to shift at a constant speed under small gradient, while the motion can be slightly accelerated under large gradient due to the broadened wall width during the motion. Furthermore, for a nonzero angular momentum, the Walker breakdown gradient could be modulated by utilizing a second anisotropy and the interfacial Dzyaloshinskii-Moriya (DM) interaction. These results provide useful information for future material design and spintronic applications.

II. ANALYTICAL ANALYSIS AND NUMERICAL SIMULATION

We investigate theoretically the domain wall motion for ferrimagnets such as rare-earth and transition-metal compounds, whose magnetic structure is depicted in Fig. 1(a), where the spins of two inequivalent sublattices are coupled antiferromagnetically [34]. We set $\mathbf{n}_{1,2}(\mathbf{r},t)$ ($\mathbf{n}_1 = -\mathbf{n}_2$), $\mathbf{M}_{1,2}(\mathbf{M}_{1,2} = M_{1,2}\cdot\mathbf{n}_{1,2})$, $\gamma_{1,2}$, $g_{1,2}$, and $\alpha_{1,2}$ to be the local unit vector at time t and position $\mathbf{r}$, magnetization moment, gyromagnetic ration, Landé g factor, and Gilbert damping constant of the two sublattices. Thus, the spin density of the sublattice i is given by $s_i = M_i/\gamma_i$ with $\gamma_i = g_i\mu_B/\hbar$, where μ_B is the Bohr magneton. It is noted that the net magnetization $\mathbf{M} = \mathbf{M}_1 + \mathbf{M}_2$ is nonzero at T_A where the net angular momentum $\delta_s = s_1 - s_2 = 0$ because of the different Landé g factors between the two sublattices.

A. Analytical treatment

Following the collective coordinate approach, the low-temperature magnetic dynamics of the FiM model is described by the Lagrangian density $L = L_B - U$ with the spin Berry phase L_B and the potential-energy density U [19,35]. In detail, the Berry phase is associated with the staggered spin density $s = (s_1 + s_2)/2$ and the net spin density δ_s, which can be described by [18,19,35]

$$L_B = s\dot{\mathbf{n}}\cdot(\mathbf{n}\times\mathbf{m}) + \delta_s\mathbf{a}(\mathbf{n})\cdot\dot{\mathbf{n}}, \tag{1}$$

where $\mathbf{n} \equiv (\mathbf{n}_1 - \mathbf{n}_2)/2$, and $\mathbf{m} \equiv (\mathbf{n}_1 + \mathbf{n}_2)/2$, $\dot{\mathbf{n}}$ represents the derivative with respect to time, and $\mathbf{a}(\mathbf{n})$ is the vector potential generated by a magnetic monopole of unit charge satisfying $\nabla_{\mathbf{n}}\times\mathbf{a} = \mathbf{n}$. The potential-energy density is given by

$$U = \frac{A_{\rm ex}}{2}(\nabla\mathbf{n})^2 + \frac{\mathbf{m}^2}{2\chi} - \frac{K(z)}{2}n_z^2 - \frac{k}{2}n_x^2 + \frac{D}{2}\mathbf{e}_y\cdot(\mathbf{n}\times\partial_z\mathbf{n}). \tag{2}$$

Here, the first and second terms are the inhomogeneous and homogeneous exchange energies, where $A_{\rm ex} > 0$ is the exchange stiffness and χ is the magnetic susceptibility. The third term is the easy-axis anisotropy along the z axis (nanowire axis) with positive K, which changes linearly with the z coordinate $K(z) = K_0 - z(dK/dz)$. The fourth term is the so-called second anisotropy or intermediate anisotropy defined along the x axis with $k > 0$, and this anisotropy should be weaker than the easy-axis anisotropy along the z axis. The last term is the interfacial DM interaction with $D > 0$ and $\mathbf{e}_y$ is the unit vector in the y direction. To obtain a more explicit expression of the Lagrangian density, we replace $\mathbf{m}$ with $\mathbf{m} = s\chi\dot{\mathbf{n}}\times\mathbf{n}$ [36,37] and obtain

$$L = \frac{\rho}{2}\dot{\mathbf{n}}^2 + \delta_s\mathbf{a}(\mathbf{n})\cdot\dot{\mathbf{n}} - \frac{A_{\rm ex}}{2}(\nabla\mathbf{n})^2 + \frac{K}{2}n_z^2 + \frac{k}{2}n_x^2 - \frac{D}{2}\mathbf{e}_y\cdot(\mathbf{n}\times\partial_z\mathbf{n}), \tag{3}$$

where $\rho \equiv s^2\chi$ parametrizes the inertia of dynamics. The dissipative dynamics can be described by introducing the Rayleigh function density $R = s_\alpha\dot{\mathbf{n}}^2/2$, with $s_\alpha = \alpha_1 s_1 + \alpha_2 s_2$

TABLE I. Parameters chosen for the simulation.

Parameter	1	2	3	4	5	6	7
M_1	1.13	1.12	1.11	1.1	1.09	1.08	1.07
M_2	1.06	1.04	1.02	1.0	0.98	0.96	0.94
δ_s	−0.03273	−0.0218	−0.0109	0	0.0109	0.0218	0.03273

accounting for the energy and spin loss due to the magnetic dynamics [38].

Now we discuss the low-energy dynamics of the FiM domain wall. Following the earlier work, we introduce two collective coordinates, the position $q(t)$ and azimuthal angle $\phi(t)$ in Eq. (3), to characterize the FiM domain wall under an anisotropy gradient. We consider the Walker ansatz [39] for the domain wall profile: $\mathbf{n}(z,t) = (\mathrm{sech}[(z-q)/\lambda]\cos\phi, \mathrm{sech}[(z-q)/\lambda]\sin\phi, \tanh[(z-q)/\lambda])$, where λ is the domain wall width. After applying the Euler-Lagrange equation, we obtain the equations of motion for the two coordinates:

$$M\ddot{q} + G\dot{\phi} + M\dot{q}/\tau = F, \tag{4}$$

$$I\ddot{\phi} - G\dot{q} + I\dot{\phi}/\tau = k_0 \sin\phi\cos\phi + D_0 \sin\phi, \tag{5}$$

where $M = 2\rho A/\lambda$ is the mass, with A the cross-sectional area of the domain wall, $I = 2\rho A\lambda$ is the moment of inertia, $G = 2\delta_s A$ is the gyrotropic coefficient, $\tau = \rho/s_\alpha$ is the relaxation time, $F = (4A\lambda)(dK/dz)$ is the force exerted by an anisotropy gradient, $k_0 = 2k\lambda A$, and $D_0 = \pi DA/2$.

A specific solution to Eqs. (4) and (5) for $k = D = 0$ gives the domain wall velocity v and domain wall plane precession speed:

$$v = \frac{2\lambda^2}{\delta_s^2/s_\alpha + s_\alpha}\frac{dK}{dz}, \tag{6}$$

$$\dot{\phi} = \frac{\delta_s}{s_\alpha \lambda} v. \tag{7}$$

Equation (6) shows that velocity v increases linearly with dK/dz and reaches the maximum at the angular momentum compensation point T_A, where δ_s vanishes ($\delta_s \sim 0$). To illustrate that this velocity can be high in real materials, one gives a crude estimation of v by taking the well-known FiM compound GdFeCo as an example [19,24,26]. Setting the internal parameter exchange stiffness $A_{\mathrm{ex}} = 50\,\mathrm{pJ/m}$, anisotropy constant at high anisotropy and $K_0 = 0.5\,\mathrm{MJ/m^3}$, the lattice size $a = 0.4\,\mathrm{nm}$, $M_1 = 440\,\mathrm{kA/m}$, $M_2 = 400\,\mathrm{kA/m}$, $\alpha_1 = \alpha_2 = 0.01$, $g_1 = 2.2$, and $g_2 = 2.0$, one obtains a wall motion velocity $v \sim 1.2\,\mathrm{km/s}$ at the compensation point under an anisotropy gradient $dK/dz = 300\,\mathrm{GJ/m^4}$, comparable to the current- and field-driven motions for antiferromagnetic domain wall motions. Furthermore, as shown in Eq. (7), the domain wall plane rotates with the domain wall propagation without any favored orientation due to $k = 0$, which is closely dependent on δ_s.

B. Numerical calculation

In order to check the validity of the above analytical treatment, we also perform the numerical simulations based on the atomistic LLG equation. Here, the corresponding one-dimensional discrete Hamiltonian is given by [40]

$$H = J\sum_i \mathbf{S}_i \cdot \mathbf{S}_{i+1} - \sum_i K_i \left(S_i^z\right)^2 - K_x \sum_i \left(S_i^x\right)^2 + \sum_i \boldsymbol{D} \cdot (\mathbf{S}_i \times \mathbf{S}_{i+1}), \tag{8}$$

where the first term is the exchange interaction with $J = 1$, $\mathbf{S}_i$ is the normalized spin moment vector at lattice site i. For simplicity, only the interaction between the nearest neighbors is considered, and the exchanges between further neighbors hardly affect our main conclusion. The second term is the anisotropy energy with the easy axis along the z direction, and the anisotropy constant at site i is described by $K_i = K_0 - ia(\Delta K)$, where ΔK describes the anisotropy gradient magnitude and a is the lattice constant. The third term is the second anisotropy K_x along the x axis, and the last term is the DM interaction with $\boldsymbol{D} = (0, D_y, 0)$.

Then, the dynamics is investigated by solving the stochastic LLG equation [41–43]:

$$\frac{\partial \mathbf{S}_i}{\partial t} = -\frac{\gamma_i}{M_i(1+\alpha_i)^2}\mathbf{S}_i \times [\mathbf{H}_i + \alpha_i(\mathbf{S}_i \times \mathbf{H}_i)], \tag{9}$$

where $\mathbf{H}_i = -\partial H/\partial \mathbf{S}_i$ is the effective field. Without loss of generality, we set the damping constants $\alpha_1 = \alpha_2 = 0.01$ and the gyromagnetic ratios $\gamma_1 = 1.1$ and $\gamma_2 = 1.0$, corresponding to the Landé g factors $g_1 = 2.2$ and $g_2 = 2.0$ for the two sublattices [44].

To investigate the dynamics in the vicinity of the momentum compensation point, several sets of (M_1, M_2) are employed, as listed in Table I. Unless stated elsewhere, the LLG simulations are performed on $1 \times 1 \times 400$ lattices with open boundary conditions using the fourth-order Runge-Kutta method with a time step $\Delta t = 1.0 \times 10^{-4}\,\mu_s/J\gamma_{\mathrm{eff}}$, where μ_s is the saturation moment and $\gamma_{\mathrm{eff}} = (\gamma_1 + \gamma_2)/2$. After a sufficient relaxation of the domain structure, the anisotropy gradient is applied to drive the domain wall motion, as schematically depicted in Fig. 1(a).

As a matter of fact, a comparison between the analytical treatment and the atomic model can be useful in a qualitative sense. It is seen from the atomistic model that various torques act on the wall spins [16]. The two spins neighboring the central wall spin deviate differently from the easy axis with $\theta_1 > \theta_2$, resulting in the net damping torque Γ^d from the exchange interaction on the central spin, as depicted in Fig. 1(b). The damping torques $\Gamma^d \sim -\mathbf{S} \times (\mathbf{S} \times \mathbf{H})$ point in an opposite direction on the two sublattices and drive the wall motion. Moreover, the precession torques $\Gamma^p \sim -\mathbf{S} \times \mathbf{H}$ pointing in the same direction on the two sublattices are unequal in magnitude in the case of $\delta_s \neq 0$, resulting in the precession of the wall plane with the wall propagation, in

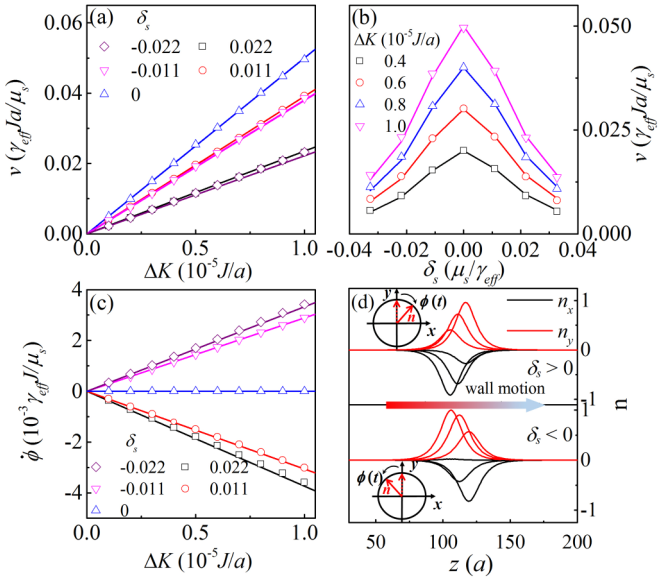

FIG. 2. The simulated (empty points) and calculated (solid lines) velocities as functions of (a) ΔK for various δ_s, and (b) δ_s for various ΔK for $K_0 = 0.01$. (c) The simulated (empty points) and calculated (solid lines) angular velocities of the wall plane as functions of ΔK for various δ_s, and (d) the evolutions of the local n_x and n_y for $\delta_s > 0$ (top half) and $\delta_s < 0$ (bottom half). The rotations of the wall plane are shown in the insert of (d).

agreement with Eq. (7). For $\delta_s = 0$, torques Γ^p on the two sublattices are equal, and the domain wall plane is fixed.

Thus, the fast domain wall motion and the precession of the wall plane in ferrimagnets are theoretically revealed and qualitatively confirmed by the atomic model simulations. Subsequently, we present the analytically derived and numerically calculated results to demonstrate the quantitative consistence between the analytical derivation and atomistic simulation and, more importantly, to unveil the FiM dynamics in detail.

III. RESULTS AND DISCUSSION

A. Domain wall dynamics

We first present the domain wall dynamics by discussing the wall velocity and precession speed, respectively, as a function of the anisotropy gradient. Figure 2(a) shows the numerically simulated (empty points) and Eq. (6)-based calculated (solid lines) wall velocity v as a function of ΔK for various δ_s and $K_0 = 0.01J$, $K_x = 0$, and $D_y = 0$. It is seen that the simulated data fit the calculations perfectly, confirming the validity of the analytical treatment. Here, two issues deserve highlighting. First, the driving torque increases with the increasing ΔK, which significantly enhances the wall motion speed. Specifically, v increases linearly with ΔK, noting that here only the low-anisotropy gradient is considered, and the domain wall width is hardly changed during the motion. Second, for a fixed ΔK, v increases with decreasing magnitude of δ_s and reaches the maximum at the angular momentum compensation point $\delta_s = 0$, as clearly shown in Fig. 2(b), where $v(\delta_s)$ curves for various ΔK are presented.

We then discuss the domain wall plane precession which appears for a nonzero δ_s in accompanying with the wall motion, as shown in Fig. 2(c), where the angular velocity $(d\phi/dt)$ of the plane as a function of ΔK is plotted. Also, two issues are highlighted. First, the angular velocity increases linearly with ΔK or the wall speed v. In comparison with the dynamics for $\delta_s = 0$, where the domain wall plane is fixed, the wall plane precession leads to additional energy dissipation, resulting in the low wall mobility for nonzero δ_s under the same ΔK. Second and more interestingly, the precession direction of the wall plane depends on the sign of δ_s. Specifically, the wall plane precesses clockwise around the easy axis for $\delta_s > 0$, while it precesses counterclockwise for $\delta_s < 0$, as clearly shown in Fig. 2(d), where the x and y components of local quantity $\mathbf{n}$, n_x and n_y, are presented at various times for $\delta_s > 0$ (top half) and $\delta_s < 0$ (bottom half). With the wall motion, opposite precession directions are clearly observed in the two cases, consistent with the theoretical prediction in Eq. (7).

So far, the anisotropy-gradient-driven domain wall motion in the vicinity of the angular momentum compensation point of ferrimagnets has been clearly uncovered in our theoretical analysis and LLG simulations. In experiments, the anisotropy gradient could be induced by tuning the electric field on particular heterostructures and efficiently drives the domain wall motion, generating Joule heat much less than the electrical-current-related methods. Thus, the proposed method in the work is expected to require low power consumption and is highly efficient, which is essential for future spintronic applications.

B. Roles of internal parameters

Based on the good consistency between analytical analysis and numerical calculations, one is able to discuss the roles of various internal parameters. An unveiling of these roles would be highly appreciated for practical applications, including materials selection, device geometry design, and performance optimization.

First, the anisotropy constant K_0 determines the wall width λ, which can be estimated by $a(J/2K_0)^{1/2}$ and in turn affects the wall speed, which increases with λ as demonstrated in Eq. (6). Thus, contrary to ΔK, a large K_0 results in a small λ and makes the wall motion slow, as confirmed in our simulations. In Fig. 3(a), the simulated and calculated speeds as functions of K_0 for various ΔK at the angular

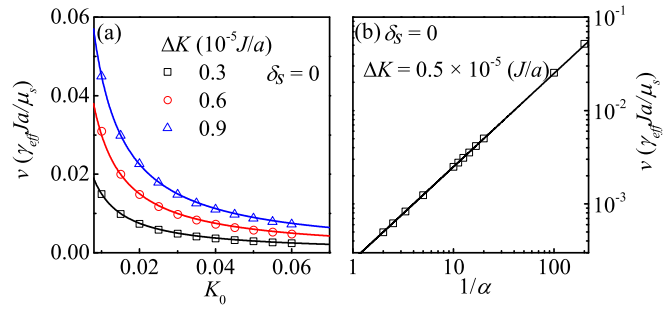

FIG. 3. The simulated (empty points) and calculated (solid lines) velocities at the momentum compensation point as functions of (a) K_0 for various value of ΔK for $\alpha = 0.01$ and (b) $1/\alpha$ for $K_0 = 0.01J$ and $\Delta K = 0.5 \times 10^{-5}\,J/a$.

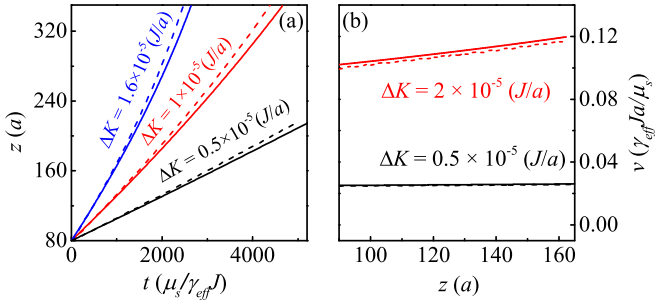

FIG. 4. The simulated (dashed lines) and calculated (solid lines) (a) evolutions of the wall positions for various ΔK and (b) instantaneous speed for various ΔK.

momentum compensation point are plotted, not only showing the excellent consistency between the simulation and analytical derivation but also clearly revealing that the anisotropy magnitude enables a slow wall motion. In addition, an enhanced damping term always reduces the wall mobility [45,46], and v decreases with the increase of the damping constant α. As a matter of fact, v linearly increases with $1/\alpha$, as shown in Fig. 3(b), which presents the simulated and calculated v as functions of $1/\alpha$ at $\delta_s = 0$ for fixed K_0 and ΔK.

In the above analysis, the wall width λ is simply set to be unchanged during the wall motion, which well describes the case of a very low anisotropy gradient. However, when the wall shifts under a high gradient, the wall is considerably enlarged, resulting in an accelerated domain wall motion. This phenomenon has been also observed in our simulations (dashed lines) and calculations (solid lines) in Fig. 4, which gives the evolution of the wall position [Fig. 4(a)] and the local wall velocity [Fig. 4(b)] for various ΔK at $\delta_s = 0$. In this case, the wall width could be updated to $\lambda = a(J/2K_c)^{1/2}$, with K_c the anisotropy on the wall central spin. A constant velocity is obtained under a low gradient $\Delta K \sim 0.5 \times 10^{-5}\,J/a$, while an acceleration of the wall motion under a high gradient $\Delta K \sim 2 \times 10^{-5}\,J/a$ is clearly observed.

Second, the intermediate anisotropy K_x could be non-negligible in some FiM materials and affects the wall motion. Subsequently, we check the effect of K_x on the dynamics of the domain wall in ferrimagnets. The time evolutions of the wall position for various K_x for $\delta_s = 0.022$ are presented in Fig. 5(a), which exhibits three types of wall motion [16]. As discussed above, the wall has no favored orientation for $K_x = 0$ and rotates continuously and moves constantly with a reduced speed. The consideration of the intermediate anisotropy suppresses the rotation of the wall plane, and in turn significantly affects the wall motion. In the case of the small anisotropy of $K_x = 2.5 \times 10^{-5}\,J$, the Walker breakdown occurs under the anisotropy gradient ΔK larger than the threshold value $\Delta K_{\rm WB}$. Here, the Walker breakdown gradient $\Delta K_{\rm WB}$ can be estimated by $K_x s_\alpha/4\delta_s\lambda$ [47,48]. In the case of high anisotropy $K_x = 10 \times 10^{-5}\,J$, the precession of the domain wall is completely suppressed for the considered ΔK, resulting in wall motion with a maximal velocity. On the other hand, the wall motion at the angular momentum compensation point $\delta_s = 0$ where no precession of the wall is available is independent of the anisotropy K_x, as clearly shown

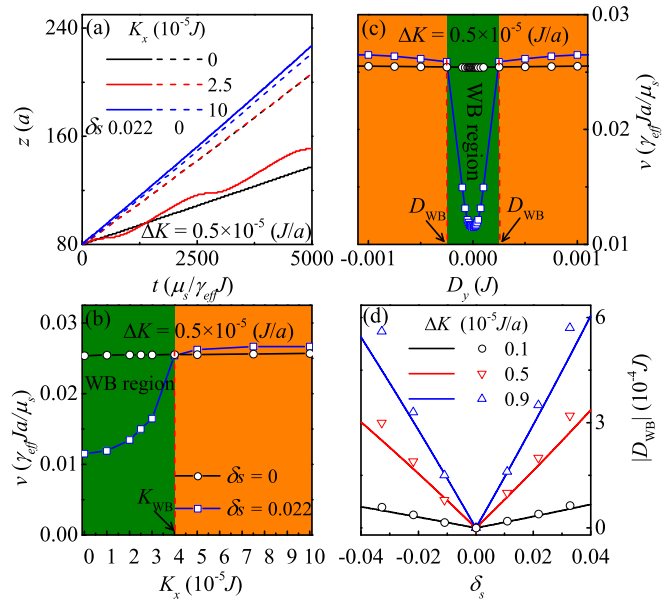

FIG. 5. For $\Delta K = 0.5 \times 10^{-5}\,J/a$, the simulated (a) evolutions of the wall position for various K_x for $\delta_s = 0$ (dash line) and $\delta_s = 0.022$ (solid line), and mean velocities as functions of (b) K_x and (c) D_y for $\delta_s = 0$ (black line) and $\delta_s = 0.022$ (blue line). The Walker breakdown regions are shown with green color. (d) The simulated (empty points) and calculated (solid lines) $|D_{\rm WB}|$ as a function of δ_s for various ΔK.

in Fig. 5(b), which presents the mean velocity of the domain wall as a function of K_x for $\delta_s = 0$ and $\delta_s = 0.022$. Moreover, for a fixed gradient ΔK below the Walker breakdown $\Delta K_{\rm WB}$, $\delta_s = 0.022$ is with a magnetization smaller than $\delta_s = 0$, and the domain wall motion for $\delta_s = 0.022$ is slightly faster than $\delta_s = 0$.

Third, a DM interaction could be induced at the interface between the heavy metal and ferrimagnet and modulated efficiently through an elaborate heterostructure design. Similarly, the interfacial DM interaction $\boldsymbol{D} = D_y(0, 1, 0)$ also suppresses the precession of the wall plane and speeds up the wall motion below $\Delta K_{\rm WB}$. In Fig. 5(c), the simulated velocities as a function of D_y for $\delta_s = 0$ and $\delta_s = 0.022$ for $\Delta K = 0.5 \times 10^{-5}\,J/a$ is plotted, revealing the critical DM interactions $D_{\rm WB}$, which can be given by $|D_{\rm WB}| = 8\delta_s\lambda^2 \times \Delta K/\pi s_\alpha$ for nonzero δ_s [26,47,48]. Under a fixed ΔK, the Walker breakdown occurs for $|D_y| < |D_{\rm WB}|$ while vanishing for $|D_y| > |D_{\rm WB}|$. The simulated $|D_{\rm WB}|$ (empty points) as a function of δ_s for various ΔK is presented in Fig. 5(d), well in consistency with the theoretical derivation (solid lines). Thus, this prediction could be used to improve the Walker breakdown field and to enhance the domain wall mobility, which is very meaningful for spintronic applications.

Thus, the domain wall motion depending on the internal parameters has been clearly unveiled, which definitely provides useful information for future material selection and device design. For example, high domain wall mobility could be available in ferrimagnet with not too large K_0 and considerable second anisotropy, as suggested in our calculations. Moreover, a large DM interaction generated in the interface between heavy metals and a ferrimagnet significantly improves the

Walker breakdown field and ensures the fast domain wall motion. Of course, the predictions given here deserve to be checked in further experiments.

IV. CONCLUSION

To summarize, we have studied analytically and numerically the dynamics of the domain wall in ferrimagnets driven by the magnetic anisotropy gradient. The wall moves towards the low-anisotropy side to release the free energy and reaches to a maximal velocity at the angular momentum compensation point which exhibits the antiferromagnetic dynamics. Moreover, the net spin angular momentum determines not only the wall velocity but also the precession direction of the domain wall plane. Furthermore, for nonzero net angular momentum, Walker breakdown occurs under a critical anisotropy gradient, which is enhanced by introducing the intermediate anisotropy and interfacial DM interaction. This work unveils a low-power-consuming and highly efficient method of controlling the domain wall in ferrimagnets, benefiting future experiment designs and spintronic applications.

ACKNOWLEDGMENTS

This work is supported by the Natural Science Foundation of China (Grants No. 51971096 and No. 51721001), the Natural Science Foundation of Guangdong Province (Grant No. 2019A1515011028), and the Science and Technology Planning Project of Guangzhou in China (Grant No. 201904010019).

[1] T. Jungwirth, X. Marti, P. Wadley, and J. Wunderlich, Nat. Nanotechnol. **11**, 231 (2016).
[2] P. Wadley, B. Howells, J. Železný, C. Andrews, V. Hills, R. P. Campion, V. Novák, K. Olejník, F. Maccherozzi, S. S. Dhesi *et al.*, Science **351**, 587 (2016).
[3] J. Železný, P. Wadley, K. Olejník, A. Hoffmann, and H. Ohno, Nat. Phys. **14**, 220 (2018).
[4] J. Torrejon, M. Riou, F. A. Araujo, S. Tsunegi, G. Khalsa, D. Querlioz, P. Bortolotti, V. Cros, K. Yakushiji, A. Fukushima *et al.*, Nature (London) **547**, 428 (2017).
[5] P. Park, J. Oh, K. Uhlířová, J. Jackson, A. Deák, L. Szunyogh, K. H. Lee, H. Cho, H.-L. Kim, H. C. Walker *et al.*, npj Quantum Mater. **3**, 63 (2018).
[6] O. Gomonay, T. Jungwirth, and J. Sinova, Phys. Rev. Lett. **117**, 017202 (2016).
[7] T. Shiino, S. H. Oh, P. M. Haney, S. W. Lee, G. Go, B. G. Park, and K. J. Lee, Phys. Rev. Lett. **117**, 087203 (2016).
[8] V. G. Barya khtar, B. A. Ivanov, and M. V. Chetkin, Sov. Phys. Usp. **28**, 563 (1985).
[9] K. M. D. Hals, Y. Tserkovnyak, and A. Brataas, Phys. Rev. Lett. **106**, 107206 (2011).
[10] A. Qaiumzadeh, L. A. Kristiansen, and A. Brataas, Phys. Rev. B **97**, 020402(R) (2018).
[11] K. Pan, L. Xing, H. Y. Yuan, and W. W. Wang, Phys. Rev. B **97**, 184418 (2018).
[12] Z. Y. Chen, Z. R. Yan, Y. L. Zhang, M. H. Qin, Z. Fan, X. B. Lu, X. S. Gao, and J.-M. Liu, New J. Phys. **20**, 063003 (2018).
[13] E. G. Tveten, A. Qaiumzadeh, and A. Brataas, Phys. Rev. Lett. **112**, 147204 (2014).
[14] S. K. Kim, Y. Tserkovnyak, and O. Tchernyshyov, Phys. Rev. B **90**, 104406 (2014).
[15] S. K. Kim, O. Tchernyshyov, and Y. Tserkovnyak, Phys. Rev. B **92**, 020402(R) (2015).
[16] S. Selzer, U. Atxitia, U. Ritzmann, D. Hinzke, and U. Nowak, Phys. Rev. Lett. **117**, 107201 (2016).
[17] Z. R. Yan, Z. Y. Chen, M. H. Qin, X. B. Lu, X. S. Gao, and J.-M. Liu, Phys. Rev. B **97**, 054308 (2018).
[18] E. G. Tveten, T. Muller, J. Linder, and A. Brataas, Phys. Rev. B **93**, 104408 (2016).
[19] K.-J. Kim, S. K. Kim, Y. Hirata, S.-H. Oh, T. Tono, D.-H. Kim, T. Okuno, W. S. Ham, S. Kim, G. Go *et al.*, Nat. Mater. **16**, 1187 (2017).
[20] J. Finley and L. Q. Liu, Phys. Rev. Appl. **6**, 054001 (2016).
[21] R. Mishra, J. W. Yu, X. P. Qiu, M. Motapothula, T. Venkatesan, and H. Yang, Phys. Rev. Lett. **118**, 167201 (2017).
[22] N. Roschewsky, T. Matsumura, S. Cheema, F. Hellman, T. Kato, S. Iwata, and S. Salahuddin, Appl. Phys. Lett. **109**, 112403 (2016).
[23] I. Radu, K. Vahaplar, C. Stamm, T. Kachel, N. Pontius, H. A. Dürr, T. A. Ostler, J. Barker, R. F. L. Evans, R. W. Chantrell *et al.*, Nature (London) **472**, 205 (2011).
[24] S. A. Siddiqui, J. H. Han, J. T. Finley, C. A. Ross, and L. Q. Liu, Phys. Rev. Lett. **121**, 057701 (2018).
[25] L. Caretta, M. Mann, F. Büttner, K. Ueda, B. Pfau, C. M. Günther, P. Hessing, A. Churikova, C. Klose, M. Schneider *et al.*, Nat. Nanotechnol. **13**, 1154 (2018).
[26] S.-H. Oh, S. K. Kim, D.-K. Lee, G. Go, K.-J. Kim, T. Ono, Y. Tserkovnyak, and K.-J. Lee, Phys. Rev. B **96**, 100407(R) (2017).
[27] K. Cai, M. Yang, H. Ju, S. Wang, Y. Ji, B. Li, K. W. Edmonds, Y. Sheng, B. Zhang, N. Zhang, S. Liu, H. Zheng, and K. Wang, Nat. Mater. **16**, 712 (2017).
[28] R. Tomasello, S. Komineas, G. Siracusano, M. Carpentieri, and G. Finocchio, Phys. Rev. B **98**, 024421 (2018).
[29] H. Xia, C. Song, C. Jin, J. Wang, J. Wang, and Q. Liu, J. Magn. Magn. Mater. **458**, 57 (2018).
[30] C. Ma, X. Zhang, J. Xia, M. Ezawa, W. Jiang, T. Ono, S. N. Piramanayagam, A. Morisako, Y. Zhou, and X. Liu, Nano Lett. **19**, 353 (2019).
[31] C. Ching, I. Ang, W. L. Gan, and W. S. Lew, New J. Phys. **21**, 043006 (2019).
[32] L. C. Shen, J. Xia, G. P. Zhao, X. C. Zhang, M. Ezawa, O. A. Tretiakov, X. X. Liu, and Y. Zhou, Phys. Rev. B **98**, 134448 (2018).
[33] D. L. Wen, Z. Y. Chen, W. H. Li, M. H. Qin, D. Y. Chen, Z. Fan, M. Zeng, X. B. Lu, X. S. Gao, and J.-M. Liu, arXiv:1905.06695.
[34] O. A. Tretiakov, D. Clarke, G.-W. Chern, Y. B. Bazaliy, and O. Tchernyshyov, Phys. Rev. Lett. **100**, 127204 (2008).
[35] S. K. Kim, K.-J. Lee, and Y. Tserkovnyak, Phys. Rev. B **95**, 140404(R) (2017).
[36] V. S. Gerasimchuk and A. A. Shitov, Low Temp. Phys. **27**, 125 (2001).
[37] B. A. Ivanov and A. L. Sukstanski, Sov. Phys. JETP **57**, 214 (1983).

[38] H. Goldstein, C. Poole, and J. Safko, *Classical Mechanics*, 3rd ed. (Addison Wesley, Reading, MA, 2002).
[39] L. D. Landau and E. M. Lifshitz, *Electrodynamics of Continuous Media*, Course of Theoretical Physics Vol. 8 (Pergamon, Oxford, 1960).
[40] F. D. M. Haldane, Phys. Rev. Lett. **50**, 1153 (1983).
[41] N. Kazantseva, U. Nowak, R. W. Chantrell, J. Hohlfeld, and A. Rebei, Europhys. Lett. **81**, 27004 (2007).
[42] D. Landau and E. Lifshitz, Phys. Z. der Sowjetunion **8**, 153 (1935).
[43] T. L. Gilbert, IEEE Trans. Magn. **40**, 3443 (2004).
[44] J. Jensen and A. R. Mackintosh, *Rare Earth Magnetism* (Clarendon, Oxford, 1991).
[45] N. L. Schryer and L. R. Walker, J. Appl. Phys. **45**, 5406 (1974).
[46] S. Moretti, M. Voto, and E. Martinez, Phys. Rev. B **96**, 054433 (2017).
[47] Z. Y. Chen, M. H. Qin, and J.-M. Liu, Phys. Rev. B **100**, 020402(R) (2019).
[48] A. Mougin, M. Cormier, J. Adam, P. Metaxas, and J. Ferr, Europhys. Lett. **78**, 57007 (2007).